Experimental benchmarking of relative potential energy minima internuclear distances with femtometer length accuracy

Adrian Krone [1,*] Philipp Schmidt [1,2] Johannes Viehmann [1] Peter Baumgärtel [3] Dana Bloß [1] Niklas Golchert [1] Emilia Heikura [1] Catmarna Küstner-Wetekam [1] Lutz Marder [1] Yusaku Terao,[1] Andreas Hans [1] and Arno Ehresmann [1]

[1]*Institute of Physics and Center for Interdisciplinary Nanostructure Science and Technology, University of Kassel, Heinrich-Plett-Str. 40, 34132 Kassel, Germany*

[2]*European XFEL, Holzkoppel 4, 22869 Schenefeld, Germany*

[3]*Helmholtzzentrum für Materialien und Energie, Hahn-Meitner-Platz 1, 14109 Berlin, Germany*

(Received 16 October 2024; accepted 11 March 2025; published 9 April 2025)

The two-dimensional photon-excitation photon-emission (PhexPhem) map of the archetypal H_2 molecule, constructed from dispersed-fluorescence measurements after energy-scanning excitation by small-bandwidth photons, displays complete systems of its Condon diffraction bands. They originate from spontaneous radiative dissociation of individual bound electronically excited rovibronic levels, one of the most relevant processes for the destruction of H_2 in space. For the *B-X* system of electronic states, we show that specific measured spectral characteristics of individual bands are extremely sensitive to the difference ΔR of the internuclear distances, where the two potential energy curves each have their minimum. Using data from recorded H_2-PhexPhem maps, it is possible to experimentally validate the calculations of ΔR down to an accuracy of at least 50 fm. This accuracy may be used as a sensitive experimental test to calculational accuracy. It is well feasible to improve the currently achieved experimental accuracy, for an even more accurate benchmark of advanced potential energy curve calculations.

DOI: 10.1103/PhysRevResearch.7.023027

I. INTRODUCTION

One of the most peculiar characteristics of H_2 is its large probability of spontaneous radiative dissociation, a process in which bound electronically excited rovibronic levels relax by photon emission into the dissociation continuum of a lower-lying bound electronic state. The emitted radiation exhibits an oscillatory intensity variation in its spectrum as a function of emission wavelength after an excitation of a discrete bound rovibronic level of the excited electronic state. This process has been predicted already by Condon [1] who called the related spectral features diffraction bands. The oscillatory intensity variation results from the varying overlap between the bound-state nuclear probability amplitude (henceforth called nuclear wave function) of the excited electronic state with the one of the dissociation continua of the lower-lying state, whose wavelength decreases with increasing kinetic energy of the fragments, weighted by the dipole transition moment at the corresponding internuclear distances.

In Figs. 1 and 2 this process and its spectral characteristics are illustrated by calculations carried out in the present study. The *B-X* potential energy curve system with the $B\,^1\Sigma_u^+(v' = 11,\ J' = 0)$ nuclear wave function and four exemplary continuum wave functions of the ground state are plotted in Fig. 1(a). Here, *X* is the ground state of H_2 and *B* its first electronically excited state. v' describes the vibrational quantum number of the electronically excited state, and J' its rotational quantum number. The corresponding Condon band is depicted in Fig. 1(b). The same band is shown in Fig. 2(c) together with a two-dimensional map of all Condon band intensities of the H_2 *B-X* potential energy curve system. The map has been plotted in a nonlinear color scale as a function of both the energy of the photons exciting the individual rovibronic levels of the *B* state and the emitted photon energy, respectively [Fig. 2(b)]. This (monochromatized) photon-excitation (dispersed) photon-emission (PhexPhem) map is a simulated representation of the data [2] used in this work for benchmarking. Figure 2(a) shows a magnified part of the PhexPhem map containing the Condon band of Fig. 2(c) labeled P, 11, 0. The P, 11, 0 label designates transitions of the P branch ($J' - J'' = -1$) into the excited *B* state with vibrational quantum number $v' = 11$ and rotational quantum number $J' = 0$.

The first experimental evidence of the diffraction bands was reported more than 40 years after Condon's work by Dalgarno *et al.* [3], who measured dispersed photon emission spectra of H_2 and D_2 flash discharges, where a manifold of excited state levels have been populated at the same time due to broad-band excitation. Although the individual emissions of the excited levels overlap spectrally, these authors observed an undulating intensity with respect to the emission wavelength (superposed on characteristic discrete spectral lines). They attributed this observation to spontaneous radiative dissociation by comparing it to the theoretical model of

*Contact author: adrian.krone@physik.uni-kassel.de

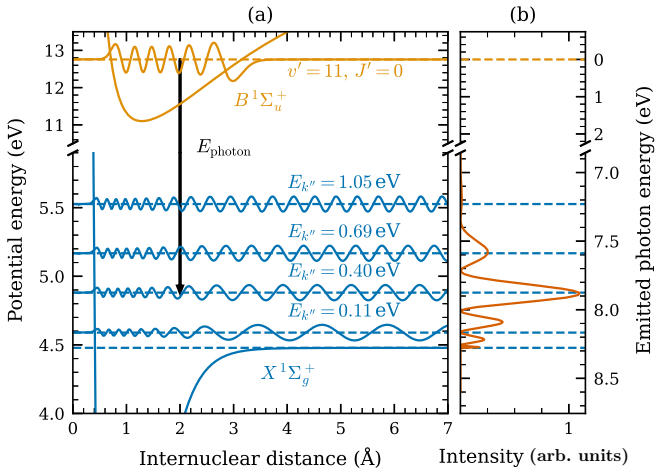

FIG. 1. (a) Calculated bound nuclear wave function of the H_2 $B\,^1\Sigma_u^+(v' = 11,\ J' = 0)$ level and continuous (dissociative) nuclear wave functions of the ground state for four selected kinetic energies of the dissociation fragments together with the corresponding potential energy curves. (b) Interpolation of the discretely calculated intensities of emitted photons as a function of emitted photon energy due to transitions into the X continuum from the upper bound level H_2 $B\,^1\Sigma_u^+(v' = 11,\ J' = 0)$.

Dalgarno and Stephens [4] using the electronic transition dipole moment of Wolniewicz [5].

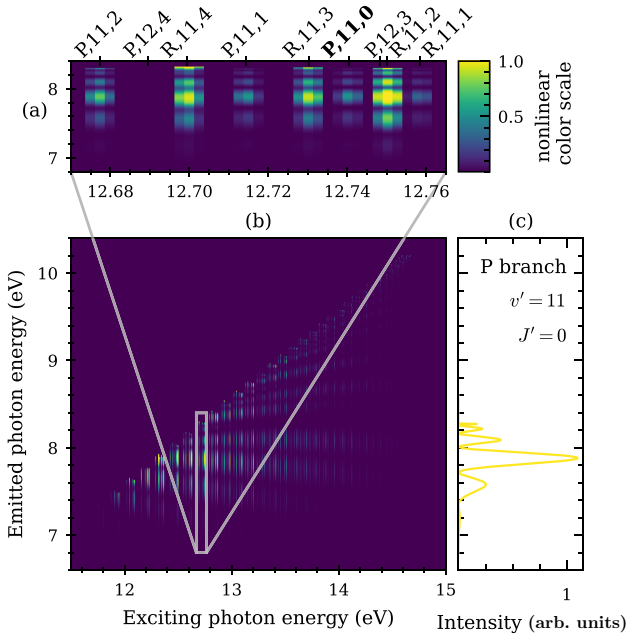

FIG. 2. (a), (b) Calculated two-dimensional photon-excitation photon-emission (PhexPhem) map convolved with a simulated experimental bandwidth of 4 meV for the excitation containing only the Condon diffraction bands from the H_2 $B\,^1\Sigma_u^+(v',\ J')$ rovibronic states radiatively dissociating into the continuum of the X state. The intensities are shown using a nonlinear color scale. (a) Magnification of the map with labels (P/Q branch,v', J') assigned to the individual Condon bands. (c) Condon band of the $B\,^1\Sigma_u^+(v' = 11,\ J' = 0)$ state excited through the P branch [same as Fig. 1(b)].

Later, by applying narrow bandwidth monochromatized synchrotron radiation, selective excitation of a few individual upper rovibronic levels of the H_2 B and C states became possible [6–8]. The observation of the subsequent dispersed photon emission at those discrete exciting-photon energies revealed differences in the diffraction bands emitted by excited levels of different rotational quantum numbers. These differences have been explained by rovibrational interactions and intensity perturbations due to rotational mixing of the B and C electronic states [8,9]. A comparison between synthetic spectra and high-resolution experimental ones obtained after electron-impact excitation [10] further substantiated the influence of rovibrational interactions and B and C state mixing in the spontaneous radiative dissociation of the B and C electronic states of H_2. Studies of radiative lifetimes by Stephens and Dalgarno [11] confirmed comparable lifetimes to bound-bound emissive decays in the slightly longer than 1 ns range. In astrophysics, this mechanism is a major pathway for destruction of H_2 in interstellar clouds, commonly referred to as Solomon process [12,13].

As the spectral features of Condon bands result from the overlap of the excited bound-state nuclear wave function with the ground state continuum (dissociative) wave function in the transition matrix elements, they are sensitive to fine details of the difference between the two involved electronic potential energy curves including (i) the difference ΔR between the two minimum potential energy internuclear distances and (ii) the precise shape of the difference potential. In this contribution we show that the observed spectral features in the Condon diffraction bands can be used to experimentally benchmark calculated ΔR of otherwise unchanged Born-Oppenheimer potential energy curves available from the literature down to a precision of 50 fm. This benchmark can be used to experimentally test calculations of electronic potential energy curves to unprecedentedly high accuracy.

II. DESCRIPTION OF THE CALCULATIONS

In the following, the concept of potential energy curves in Born-Oppenheimer approximation is used. The total molecular wave function of a diatomic molecule is then written as

$$\Psi = \psi_e(\boldsymbol{r}; R)\frac{u_v^J(R)}{R}Y_{\Lambda,J,M_J}(\vartheta, \varphi). \tag{1}$$

Here ψ_e is the electronic part of the wave function, which depends on the coordinates of all electrons (represented by $\boldsymbol{r}$) and parametrically on the internuclear distance R. The product $\frac{u_v^J(R)}{R} \times Y_{\Lambda,J,M_J}(\vartheta, \varphi)$ describes the wave function of nuclear motion with the rotational part $Y_{\Lambda,J,M_J}(\vartheta, \varphi)$ and eigenfunctions $\chi_v^J(R) = \frac{u_v^J(R)}{R}$ describing nuclear vibration and dissociation. The rotational nuclear wave function depends on the projection Λ of the electronic orbital angular momentum onto the internuclear axis, the angular momentum J of the molecular rotation and its projection M_J onto the internuclear axis. The vibrational part depends on the vibrational quantum number v and the quantum number of molecular rotation J and satisfies the radial Schrödinger

equation

$$\left\{ -\frac{\hbar^2}{2\mu}\frac{\mathrm{d}^2}{\mathrm{d}R^2} + U_{e\Lambda\Sigma}(R) - \frac{\hbar^2}{2\mu R^2}[J(J+1) - \Omega^2] \right\} \chi_v^J(R) = E_v^J \chi_v^J(R), \quad (2)$$

where $\mu = \frac{M_1 M_2}{M_1 + M_2}$ is the reduced mass of the two nuclei, E_v^J is the energy of nuclear vibration (or dissociation) and $U_{e\Lambda\Sigma}(R)$ is the electronic potential at fixed nuclei positions R with electronic angular momentum projection $\Omega = \Lambda + \Sigma$ onto the internuclear axis [Λ is the total orbital electronic angular momentum projection, Σ is the total spin angular momentum projection, Hund's case (a) is assumed]. For the B and X electronic states involved in the present study $\Omega = 0$. This equation describes discrete bound vibrational states $\chi_v^J(R)$ below the dissociation energy D_e of the respective electronic potential energy curve with energies $E_v^J < D_e$. For energies above D_e the spectrum is continuous. The respective wave functions converge towards plane waves of a free particle, are no longer bound, and represent the dissociation of the molecule. They may be characterized by the momentum of the dissociating atoms expressed in terms of the continuous wave number k, i.e., $\chi_k(R)$ with corresponding energies E_k. Using an alternative expression for the nuclear kinetic energy operator $\hat{T}_n = -\frac{\hbar^2}{2\mu}\frac{\mathrm{d}^2}{\mathrm{d}R^2} = \frac{\hat{p}^2}{2\mu}$, the Schrödinger equation for the radial nuclear wave function reads

$$\left[\frac{\hat{p}^2}{2\mu} + U_{e\Lambda=0\Sigma=0}(R) - \frac{\hbar^2}{2\mu R^2} J(J+1) \right] \chi_v^J(R) = E_v^J \chi_v^J(R). \quad (3)$$

The potential energy curves $U_{e\Lambda\Sigma}(R)$ for the electronic states of the present work have been taken for the ground state from calculations by Wolniewicz [14] and for the excited B state from calculations by Staszewska and Wolniewicz [15], which take into account a variety of corrections to increase the accuracy of the strict Born-Oppenheimer approximation. We will use these potential energy curves to illustrate the power of the suggested experimental benchmarking. Recently, new calculations of potential energy curves have been published [16–18] giving rise to a variety of potential applications of the proposed benchmarking method.

With the potential energy curves, the radial Schrödinger equation for nuclear motion has been solved numerically, by expressing its Hamiltonian as a discrete matrix $\boldsymbol{H}$ on a finite grid of internuclear distances and solving the resulting eigenvalue problem. With the obtained energies and nuclear wave functions the Condon bands have been calculated (see Appendix).

III. CONDON BAND SENSITIVITY ON THE DIFFERENCE POTENTIAL

We will now investigate how sensitively the intensity distributions of the B-X Condon bands depend on the relative distance ΔR between the minima $R_{\min}^B$ and $R_{\min}^X$ of the (otherwise unchanged) potential energy curves and evaluate whether experimental data may be used to test corresponding calculations within the necessary accuracy. To avoid influences of rotational mixing between the B and C excited electronic states we restrict the following discussion to levels with $J' = 0$. Exemplarily, Fig. 3 shows the situation for the wave functions of the $B\,^1\Sigma_u^+(v' = 3,\ J' = 0)$ (large oscillation period, bound-state wave function located largely above the potential energy well of the ground state), $B\,^1\Sigma_u^+(v' = 11,\ J' = 0)$ (intermediate oscillation period, bound-state wave function extends over the internuclear distance range of the ground-state potential energy well as well as over the dissociation continuum), and the $B\,^1\Sigma_u^+(v' = 32,\ J' = 0)$ level (small oscillation period, wave function extending widely into the dissociation potential of the ground state). As is obvious from Fig. 3, the largest sensitivity of Condon diffraction band oscillations on ΔR is expected when the oscillation periods of the two involved wave functions match over a wide range of internuclear distance. Generally, for higher v' this matching will be better for higher kinetic energies of the dissociation fragments (longer emitted photon wavelength).

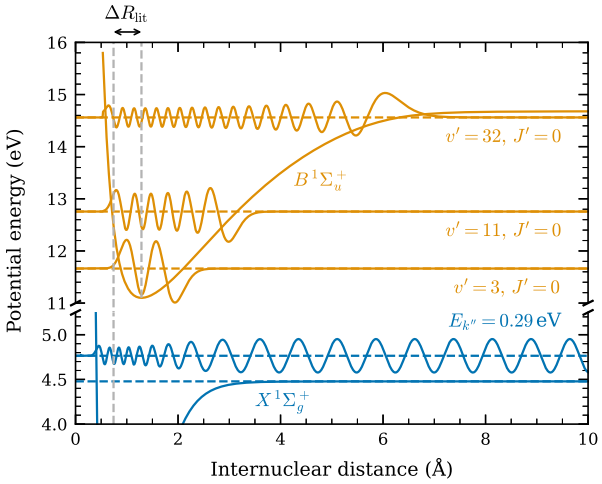

FIG. 3. Sketch to illustrate the different overlaps of bound state wave functions of the levels $(v' = 32,\ J' = 0)$, $(v' = 11, J' = 0)$, $(v' = 3, J' = 0)$ with an arbitrarily selected continuum (dissociative) nuclear wave function of the ground state with a kinetic energy of 0.29 eV.

The calculated ground-state potential energy minimum internuclear distance has been published to be $R_{\min}^X = 1.4011$ a.u. [19], corresponding to 74.14 pm. For the B state the corresponding calculated quantity has been $R_{\min}^B = 2.43$ a.u. [20], corresponding to 128.6 pm. For both quantities an uncertainty of ± 1 in the last given digit of the atomic unit value will be assumed, although no uncertainty estimates of these values in the corresponding calculations have been given. ΔR, therefore, possesses an uncertainty of the less certain value, i.e., ± 0.01 a.u., corresponding to ± 0.5 pm. We will now investigate whether experiments recording individual Condon bands are able to corroborate calculations within such a small uncertainty. In the present calculations ΔR is therefore varied around the literature value of $\Delta R_{\mathrm{lit}} = 54.46$ pm for each band and the change in the oscillation pattern is evaluated as a function of ΔR. Figure 4(a) shows exemplary results of the Condon band corresponding to emissive dissociation of the $(v' = 11,\ J' = 0)$ level of the electronic B state, calculated for potential energy minima internuclear distance differences of $\Delta R = \Delta R_{\mathrm{lit}} + \mathrm{d}\Delta R$ for $\mathrm{d}\Delta R = -0.5$ pm, 0 pm,

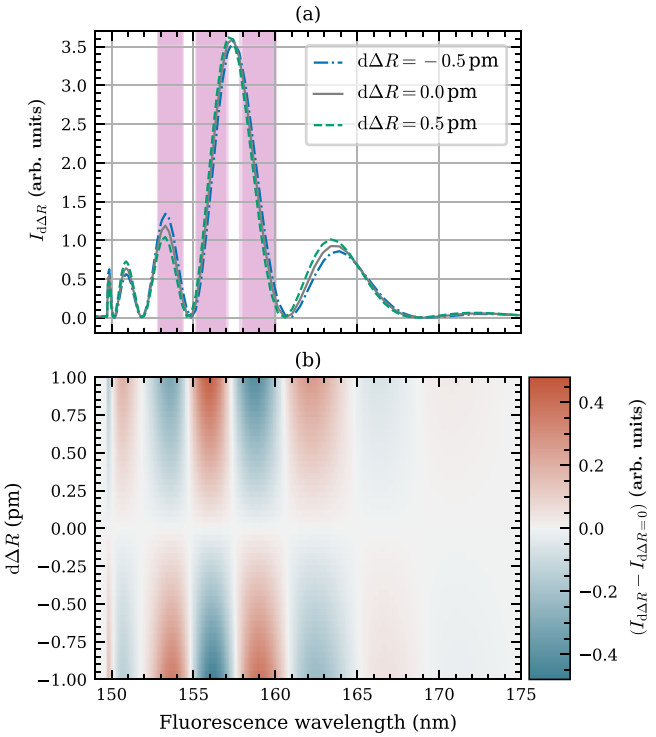

FIG. 4. (a) Calculated relative intensities as a function of emitted photon wavelength of the Condon band of radiative dissociation from the $B\,^1\Sigma_u^+(v' = 11,\ J' = 0)$ level, for potential energy minima internuclear distance differences ΔR between the X and the B state, corresponding to the literature value $\Delta R_{\text{lit}} = 54.46\,\text{pm}$ ($d\Delta R = 0.0\,\text{pm}$) (solid), for $\Delta R = 54.96\,\text{pm}$ ($d\Delta R = 0.5\,\text{pm}$) (dashed) and for $\Delta R = 53.96\,\text{pm}$ ($d\Delta R = -0.5\,\text{pm}$) (dash-dotted). The highlighted wavelength ranges are the same as in Fig. 5 for $B\,^1\Sigma_u^+(v' = 11,\ J' = 0)$. (b) Differences of the spectra with respect to the unshifted ($d\Delta R = 0\,\text{pm}$) case for shifts from $d\Delta R = -1\,\text{pm}$ to 1 pm.

and 0.5 pm. To identify for each band at which wavelengths the most sensitive effects occur, the differences of the calculated spectra between minima difference shifts of $\pm d\Delta R$ in the range $d\Delta R = -1\,\text{pm}$ to 1 pm and the spectrum expected from the literature value are shown in Fig. 4(b). For this case, the presented calculations predict relative intensity differences at specific emission wavelengths of up to 11% at a shift of ± 0.5 pm. These possible intensity differences are well suited for benchmarking the potential energy curves, because they are observable for very narrow fluorescence wavelength ranges and, therefore, do not require to include spectral and positional variations of the quantum efficiency for the detection system.

In order to showcase the method the data of Schmidt *et al.* [2] is compared to the calculations. For the Condon bands of the $B\,(v' = 8, 9, \ldots, 13,\ J' = 0)$ states a simultaneous maximum likelihood fit is performed in the most sensitive emitted photon wavelength ranges (shaded areas in Fig. 5) extracting an estimated shift $d\Delta R$ with respect to the theoretical literature value. This has been achieved by forcing the fit parameter of the shift $d\Delta R$ to be the same for all bands during the optimization. All other fit parameters are not shared between the bands and adjust the intensity scaling (one scaling factor for each individual Condon band). The uncertainties shown

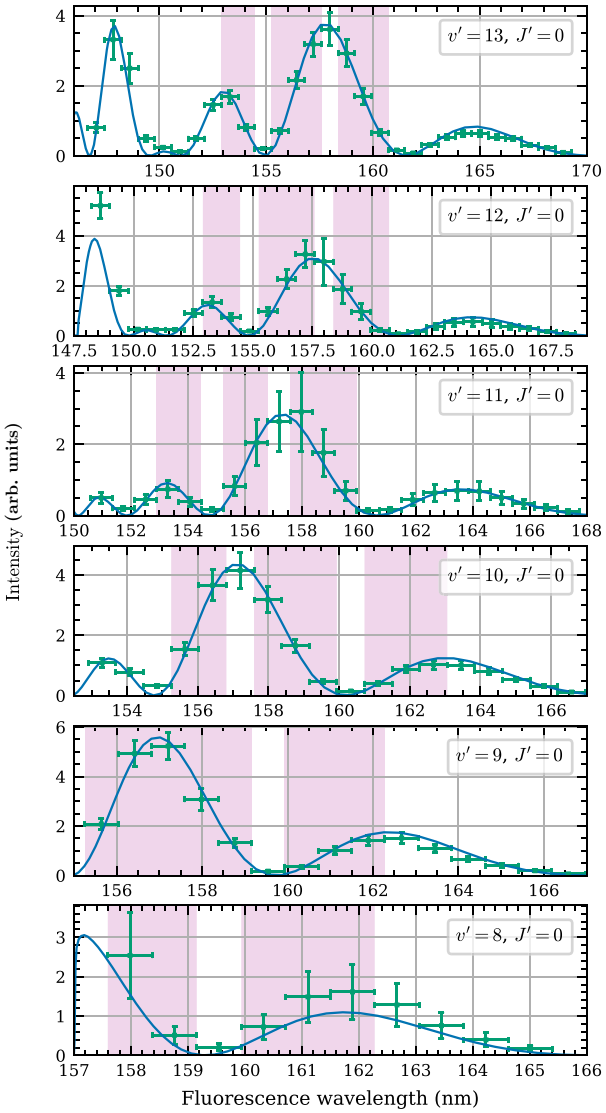

FIG. 5. Simultaneous maximum likelihood fit (solid lines) of the calculated Condon diffraction bands to the experimental data of Schmidt *et al.* [2] (squares) with only a joint shift $d\Delta R$ and band-individual intensity scaling factors. The vertical error bars include the Poisson uncertainty and uncertainties propagated from the calibration of the exciting-photon energy. The bin widths (horizontal error bars) are approximately the 1σ uncertainty of the detector wavelength calibration. Only the highlighted ranges are included in the fit.

in Fig. 5 (vertical error bars) are dominated by uncertainties of the calibration of the exciting-photon energy and include the Poisson uncertainty of each bin. The horizontal error bars represent the bin widths, which approximately correspond to the 1σ uncertainty of the wavelength calibration of the detector. Systematic errors from the normalization to the experiment conditions and detector efficiencies are not included and are regarded as negligible. The obtained shift between the B and X potential energy curves that fits the experimental data best is

$$d\Delta R = 0.07(5)\,\text{pm}. \tag{4}$$

The benchmarking with the available experimental data results in a suggested shift of the potential energy curves by 0.07(5) pm towards longer internuclear distance with respect to the literature value. The suggested shift, however, is within the assumed uncertainty of the used potential energy curve calculations [14,15].

IV. CONCLUSION AND OUTLOOK

This study has evaluated the sensitivity of spectral intensity features in individually observed Condon bands of the H_2 B-X system on variations of ΔR, the difference between the internuclear distances of the minima of the two involved potential energy curves. The analysis strategy for benchmarking potential energy curve calculations has been demonstrated with available experimental data [2] using artificially introduced shifts $\mathrm{d}\Delta R$ of published potential energy curves [14,15]. We show that an experimental benchmarking of $\mathrm{d}\Delta R$ is possible down to an unprecedented accuracy of 50 fm, which is in the same order of magnitude as recently achieved by Rupprecht *et al.* [21] for vibrations in SF_6 molecules. With optimized measurements it is well possible to largely increase the current accuracy. This will allow an even more sensitive benchmark of potential energy curves calculation procedures of diatomics down to length accuracies on the scale of the radius of the proton. As this study has been restricted on Condon diffraction bands starting from $J' = 0$ levels, nonadiabatic rotational coupling between the B- and C-electronic states [9,22] can be neglected. The influence of rotational coupling between these states will be investigated in a separate study on Condon diffraction bands starting at levels with $J' > 0$ and promises to further extend the capabilities of the presented method. Finally, using the same method and modifying the shape of calculated potential energy curves, we expect experimental hints of long-range interactions between the two dissociating H atoms.

ACKNOWLEDGMENTS

The staff of BESSY II is gratefully acknowledged for hands-on help and support during the beam times, particularly for keeping the U125-2 NIM beam line in excellent shape. This work was supported by the German Federal Ministry of Education and Research (BMBF) (Project No. 05K19RK2) and Deutsche Forschungsgemeinschaft (Project No. 512040818).

APPENDIX: CALCULATION OF THE CONDON DIFFRACTION BANDS

Some details of the code have been described in Ref. [23]. Briefly, the radial Schrödinger equation of nuclear motion (3) has been solved using a grid discretizing the nuclear coordinate R in its range between $[R_{\min},\ R_{\max}]$ into an odd number of N equidistant points located at

$$R_n = R_{\min} + (n-1)\mathrm{d}R, \quad n = 1, 2, \ldots, N \tag{A1}$$

with a distance of

$$\mathrm{d}R = \frac{R_{\max} - R_{\min}}{N-1}. \tag{A2}$$

$R_{\min}$ has been chosen to be $\frac{a_0}{2}$ (a_0 = Bohr radius) and $R_{\max} = 20 \times a_0$ in view of the rather wide electronic potential of the B state. The individual matrix elements H_{nm} of the Hamilton operator have been obtained using the Fourier grid Hamiltonian (FGH) method [24,25] for discretized grids in position and momentum space. As the Hamiltonian separates into its three terms $\boldsymbol{H} = \boldsymbol{H}_{\mathrm{kin}} + \boldsymbol{H}_{\mathrm{pot}} + \boldsymbol{H}_{\mathrm{rot}}$, the matrix elements of the latter two terms may simply be expressed as diagonal matrices in position space. The nuclear kinetic energy term, however, is solved by the FGH method in momentum space. Using the de Broglie relation $p = \hbar k$ the momentum is expressible by the wave number k, for which also a grid of values

$$k_n = A_n \frac{2\pi}{R_{\max} - R_{\min}} \tag{A3}$$

can be introduced, where the odd number of integer values

$$A_n = \frac{2n - N - 1}{2}, \quad n = 1, 2, \ldots, N \tag{A4}$$

may be regarded as the components of an N-dimensional vector $\boldsymbol{A}$. The used basis set can be expressed as an $N \times N$ matrix $\boldsymbol{\phi}$ with elements

$$\phi_{mn} = \frac{1}{\sqrt{2\pi}} \exp\left(2\pi \mathrm{i} A_n \frac{m}{N}\right), \tag{A5}$$

where the discretized k_n and R_m vary along its columns and rows. In this way the matrix elements of the nuclear kinetic energy operator are just matrix operations between $\boldsymbol{\phi}$ and vector $\boldsymbol{A}$:

$$\boldsymbol{H}_{\mathrm{kin}} = \frac{\boldsymbol{p}^2}{2\mu} = \frac{\hbar^2}{2\mu} \frac{1}{(R_{\max} - R_{\min})^2} \boldsymbol{\phi}^* \boldsymbol{A}^\top \boldsymbol{A} \boldsymbol{\phi}. \tag{A6}$$

The eigenvalues E_v^J and eigenvectors $\boldsymbol{\chi}_{\mathrm{discr}}^{v,J}(R)$ of the final matrix $\boldsymbol{H}$ are numerically determined [26] with the QR algorithm for Hermitian matrices [27]. The eigensystem contains both bound rovibrational levels up to the dissociation limit as well as unbound continuum levels understood as discrete samples of the continuum.

The bound-state wave functions $\chi^J_{v \leqslant v_{\mathrm{limit}}}(R)$ (v_{limit} is the quantum number of the energetically highest bound state) need to be square integrable, i.e., with a proper normalization factor the condition

$$\int_{-\infty}^{\infty} \left|\chi^J_{v \leqslant v_{\mathrm{limit}}}(R)\right|^2 \mathrm{d}R = 1 \tag{A7}$$

is fulfilled. For the discrete approximations to the wave functions this translates to

$$\chi^J_{v \leqslant v_{\mathrm{limit}}}(R) \approx \frac{\chi_{\mathrm{discr}}^{v \leqslant v_{\mathrm{limit}},J}(R)}{\sqrt{\sum_i \chi_{\mathrm{discr}}^{v \leqslant v_{\mathrm{limit}},J}(R_i)\mathrm{d}R}}. \tag{A8}$$

Nuclear wave functions describing the dissociation continuum $\chi_{\mathrm{discr}}^{v > v_{\mathrm{limit}},J}(R)$ cannot be normalized in the same way as the discrete bound ones. Their probability densities extend to $R \to \infty$ with finite values. Instead, if their eigenvalues grow exponentially with their vibrational quantum number v, i.e., they follow an exponential function with parameters E_0, K, γ of the form

$$E_v^J = E_0 + K\mathrm{e}^{\gamma v}, \tag{A9}$$

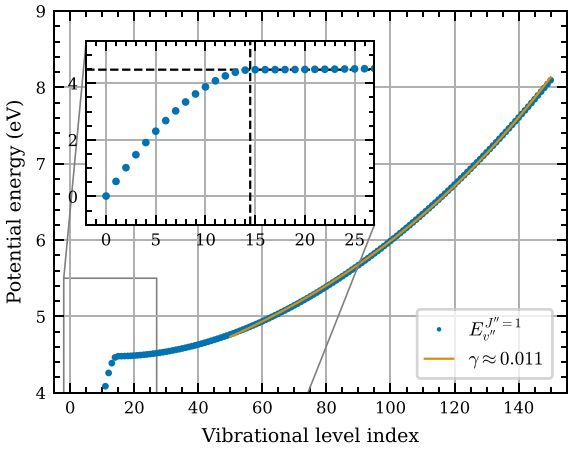

FIG. 6. Energies of vibrational levels ($J = 1$) numerically obtained as described in the text for the H_2 $X\ ^1\Sigma_g^+$ ground state. The levels $(X, v'') \leqslant (X, v_{\text{limit}} = 14)$ are bound states, while $(X, v'') > (X, v_{\text{limit}} = 14)$ describe discretized levels in the dissociation continuum. At the boundary between bound and continuum levels (dashed vertical line in inset), the energy levels (dots in inset) possess a negligible slope. The energetic spacing between the continuum levels grows exponentially with the vibrational quantum number v''.

the normalization may be performed using a density of eigenstates $\rho(E_v^J)$ around any eigenvalue E_v^J in the continuum [28]. The properly normalized wave function $\chi_{\text{discr}}^{v>v_{\text{limit}},J}(R)$ of a discretized continuum state can then be obtained from the unnormalized wavefunction $\tilde{\chi}_{\text{discr}}^{v>v_{\text{limit}},J}(R)$ by

$$\chi_{\text{discr}}^{v>v_{\text{limit}},J}(R) = \sqrt{\rho\left(E_v^J\right)} \times \tilde{\chi}_{\text{discr}}^{v>v_{\text{limit}},J}(R). \tag{A10}$$

For $\gamma < 2$, i.e., for small energetic spacings between the sampled energies, the density may be approximated by

$$\rho\left(E_v^J\right) \approx \frac{2}{E_{v+1}^J - E_{v-1}^J}. \tag{A11}$$

Using the described method, probability amplitudes have been calculated for the discretized continuum levels ($v'' = 15$, $J'' = 1$) to ($v'' = 150$, $J'' = 1$) of the H_2 $X\ ^1\Sigma_g^+$ ground state and for the bound levels ($v' = 8, J' = 0$) to ($v' = 13$, $J' = 0$) of the excited H_2 $B\ ^1\Sigma_u^+$ state. Figure 6 demonstrates the validity of the normalization of the discretized continuum levels by estimating the value $\gamma \approx 0.011$, which fulfills the condition of small energy spacing, with a least-squares fit.

For each combination of excited $B\ ^1\Sigma_u^+(v',\ J' = 0)$ and relaxed $X\ ^1\Sigma_g^+(v'',\ J'' = 1)$ states an intensity

$$I_{v''v'} \propto (E_{v'} - E_{v''})^3 \left| \int \chi_{v''} \chi_{v'} d_{XB}^{\text{e}}(R)\, \mathrm{d}R \right|^2 \tag{A12}$$

is calculated by numerically integrating the overlap (elementwise multiplication) of the two corresponding eigenvectors $\boldsymbol{\chi}_{\text{discr}}^{v''}$ and $\boldsymbol{\chi}_{\text{discr}}^{v'}$ (Franck-Condon factor) weighted with the electronic transition moments $d_{XB}^{\text{e}}(R)$ [29]. The Condon

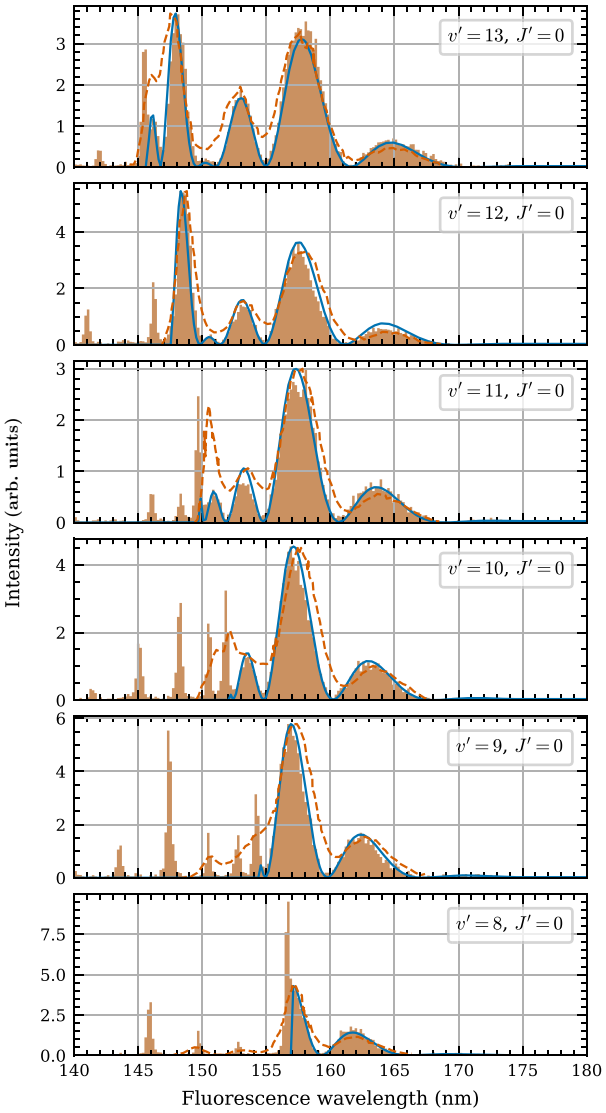

FIG. 7. Comparison between the present calculations (solid line), the experimental results, digitized from Noll and Schmoranzer [7] (dashed line), and analyzed data of the measurements of Schmidt *et al.* [2] (histogram). In the calculation only the spectral features corresponding to emissive dissociation are shown, bound-bound transitions have been omitted. The highest maxima of measured and calculated intensities have been normalized to each other for better comparison (similarly as in Ref. [7]).

diffraction bands are then obtained by linearly interpolating the discrete intensities.

The results are compared to the published measurement results digitized from the plots of Noll and Schmoranzer [7] and with our own measurements described in Schmidt *et al.* [2] (see Fig. 7). Satisfactory agreement between the calculational results and both measurements for the chosen state-selectively excited rovibronic levels of the B state has been achieved.

[1] E. U. Condon, Nuclear motions associated with electron transitions in diatomic molecules, Phys. Rev. **32**, 858 (1928).

[2] P. Schmidt, A. Knie, A. Hans, K. Hosaka, M. Ukai, M. Glass-Maujean, and A. Ehresmann, Photon-excitation

photon-emission maps (phexphem maps) with rovibronic resolution as a data base for theory and astrophysics part I: Method and first results for H_2, J. Phys. B: At. Mol. Opt. Phys. **54**, 034001 (2021).

[3] A. Dalgarno, G. Herzberg, and T. L. Stephens, A new continuous emission spectrum of the hydrogen molecule, Astrophys. J. **162**, L49 (1970).

[4] A. Dalgarno and T. L. Stephens, Discrete absorption and photodissociation of molecular hydrogen, Astrophys. J. **160**, L107 (1970).

[5] L. Wolniewicz, Theoretical investigation of the transition probabilities in the hydrogen molecule, J. Chem. Phys. **51**, 5002 (1969).

[6] H. Schmoranzer and R. Zietz, Observation of selectively excited continuous vacuum ultraviolet emission in molecular hydrogen, Phys. Rev. A **18**, 1472 (1978).

[7] T. Noll and H. Schmoranzer, Fluorescent dissociation of selectively excited rotational-vibrational states of $H_2(B, C)$ molecules, Phys. Scr. **36**, 129 (1987).

[8] H. Schmoranzer, T. Noll, E. Roueff, H. Abgrall, and R. J. Bieniek, Rotational effects in the continuous vacuum-ultraviolet fluorescence spectrum of H_2 associated with spontaneous dissociation, Phys. Rev. A **42**, 1835 (1990).

[9] H. Abgrall, F. Launay, E. Roueff, and J. Y. Roncin, Effect of rotational coupling on emission probabilities of Lyman and Werner band systems of the vacuum ultraviolet spectrum of H_2, J. Chem. Phys. **87**, 2036 (1987).

[10] H. Abgrall, E. Roueff, X. Liu, and D. E. Shemansky, The emission continuum of electron-excited molecular hydrogen, Astrophys. J. **481**, 557 (1997).

[11] T. L. Stephens and A. Dalgarno, Spontaneous radiative dissociation in molecular hydrogen, J. Quant. Spectrosc. Radiat. Transfer **12**, 569 (1972).

[12] P. M. Solomon, The absorption coefficient of quasi-molecular hydrogen, Astrophys. J. **139**, 999 (1964).

[13] T. P. Stecher and D. A. Williams, Photodestruction of hydrogen molecules in HI regions, Astrophys. J. **149**, L29 (1967).

[14] L. Wolniewicz, Relativistic energies of the ground state of the hydrogen molecule, J. Chem. Phys. **99**, 1851 (1993).

[15] G. Staszewska and L. Wolniewicz, Adiabatic energies of excited $1\Sigma u$ states of the hydrogen molecule, J. Mol. Spectrosc. **212**, 208 (2002).

[16] H. Nakashima and H. Nakatsuji, Solving the schrödinger equation of hydrogen molecule with the free complement-local schrödinger equation method: Potential energy curves of the ground and singly excited singlet and triplet states, Σ, Π, Δ, and Φ, J. Chem. Phys. **149**, 244116 (2018).

[17] M. Siłkowski, M. Zientkiewicz, and K. Pachucki, Accurate Born-Oppenheimer potentials for excited Σ^+ states of the hydrogen molecule, in *New Electron Correlation Methods and their Applications, and Use of Atomic Orbitals with Exponential Asymptotes*, edited by M. Musial and P. E. Hoggan, Advances in Quantum Chemistry, Vol. 83 (Academic Press, 2021), Chap. 12, pp. 255–267.

[18] M. Siłkowski and K. Pachucki, Born–Oppenheimer potentials for Π, Δ, and Φ states of the hydrogen molecule, Mol. Phys. **120**, e2062471 (2022).

[19] L. Wolniewicz, Nonadiabatic energies of the ground state of the hydrogen molecule, J. Chem. Phys. **103**, 1792 (1995).

[20] L. Wolniewicz, Lowest order relativistic corrections to the energies of the $B^1\Sigma_u$ state of H_2, Chem. Phys. Lett. **233**, 647 (1995).

[21] P. Rupprecht, L. Aufleger, S. Heinze, A. Magunia, T. Ding, M. Rebholz, S. Amberg, N. Mollov, F. Henrich, M. W. Haverkort, C. Ott, and T. Pfeifer, Resolving vibrations in a polyatomic molecule with femtometer precision via x-ray spectroscopy, Phys. Rev. A **108**, 032816 (2023).

[22] H. Abgrall and E. Roueff, Wavelengths, oscillator strengths and transition probabilities of the H_2 molecule for Lyman and Werner systems, Astron. Astrophys. Suppl. Ser. **79**, 313 (1989).

[23] P. Schmidt, Visualizing the electronic structure of small molecules with rovibronic photon emission spectroscopy, Ph.D. thesis, University of Kassel, 2018.

[24] C. C. Marston and G. G. Balint-Kurti, The fourier grid Hamiltonian method for bound state eigenvalues and eigenfunctions, J. Chem. Phys. **91**, 3571 (1989).

[25] G. G. Balint-Kurti, C. L. Ward, and C. C. Marston, Two computer programs for solving the Schrödinger equation for bound-state eigenvalues and eigenfunctions using the Fourier grid Hamiltonian method, Comput. Phys. Commun. **67**, 285 (1991).

[26] E. Anderson, Z. Bai, C. Bischof, L. S. Blackford, J. Demmel, J. Dongarra, J. D. Croz, A. Greenbaum, S. Hammarling, A. McKenney, and D. Sorensen, *LAPACK Users' Guide* (SIAM, Philadelphia, 1999).

[27] K. Gates and W. B. G. A, Notes on TQR algorithms, J. Comput. Appl. Math. **86**, 195 (1997).

[28] A. Macías, F. Martín, A. Riera, and M. Yáañez, A practical solution to the "unknown normalization" problem, Int. J. Quantum Chem. **33**, 279 (1988).

[29] L. Wolniewicz and G. Staszewska, $^1\Sigma_u^+ \rightarrow X^1\Sigma_g^+$ transition moments for the hydrogen molecule, J. Mol. Spectrosc. **217**, 181 (2003).